Simplified CFD approach of a hollow fiber ultrafiltration system

R. Ghidossi [a], J.V. Daurelle [a], D. Veyret [a], P. Moulin [b],*

[a] IUSTI, UMR CNRS 6595, Polytech' Marseille, Technopôle de Château-Gombert, 5 rue Enrico Fermi, 13453 Marseille Cedex 13, France
[b] LPPE, UMR CNRS 6181, Université Paul Cézanne, Europôle de l'Arbois, Bâtiment Laennec, Hall C, 13545 Aix en Provence Cedex 4, France

Abstract

Pressure driven membrane filtration processes have emerged as cost effective and confirmed technologies. Ultrafiltration is used to produce drinking water. Hollow fiber membranes are used in industrial processes but there is still a need of predicting pressure drops for design and optimization purposes: to control the production of water, to anticipate problems such as the clogging of the hollow fibers and/or the module position and to consider energy consumption. This prediction could also enhance current models that calculate pressure drop using the Hagen–Poiseuille law. In this work, the flow characteristics controlling the performance of a hollow fiber membrane module are investigated numerically. The aim of this study is to determine the pressure drop in a module depending on the operating conditions and membrane characteristics: a simplified model equation is proposed. We use a commercial CFD package (FLUENT). Numerical simulation can provide a better understanding of module performance, especially for permeable wall and/or complex multi-component systems. CFD can be used to better apprehend fluid flows in complex geometries and to test the influence of process parameters. The results are compared to experimental data obtained with an industrial pilot plant: a good agreement with our relation is obtained.
© 2006 Elsevier B.V. All rights reserved.

Keywords: Computational fluid dynamics; Hollow fiber; Pressure drop; Model; Ultrafiltration

1. Introduction

Ultrafiltration is a pressure driven membrane process that can be applied to a wide variety of fields: chemical industry, food technology, pharmaceutical industry and water treatment. One of the most important ultrafiltration design is the hollow fiber configuration. Some advantages of this geometry are the low cost of investment and the high specific area unit per volume. A high number of applications have proved that membrane processes are economically attractive and useful [1]. However, problems such as membrane fouling and concentration polarization phenomena limit the use of these membrane processes, because they reduce permeate fluxes, membrane life and efficiency and they have economic repercussions [2]. The membrane can be plugged or broken, which creates disturbances in the process. These problems also impose major limitations on the application and development of membrane processes. In this paper, we present a detailed model that describes ultrafiltration membranes. Numerical simulations were run to represent the phenomenon. Various simulations were run to show the flexibility of the relation developed in this work for a wide range of inlet velocities, inlet pressures, internal diameters, permeabilities and Reynolds numbers. This simplified relation represents the flow mechanism in the module and allows the calculation of the pressure drop for all the configurations. These results were compared to experimental results.

2. Previous study

The modelling of flow with permeable walls is not recent. Several diversely complex studies started emerging a long time ago. Berman [3,4] and Yuan and Finkelstein [5] were the first to solve the Navier–Stokes equations for a laminar flow in a porous slit and in a porous tube, respectively. They assumed that the axial flow was fully developed and that the shape of the non-dimensional velocity profile was invariant with the axial distance. In order to better understand the problems of membrane processes, it is necessary to describe laminar flows in porous tubes. One of the common ultrafiltration membrane designs is the hollow fibber module in which the membrane is formed on the inside of small polymer cylinders that are then ranged in a carter as shown in Fig. 1. For example, ultrafiltration

* Corresponding author. Tel.: +33 4 42 90 85 05; fax: +33 4 42 90 85 15.
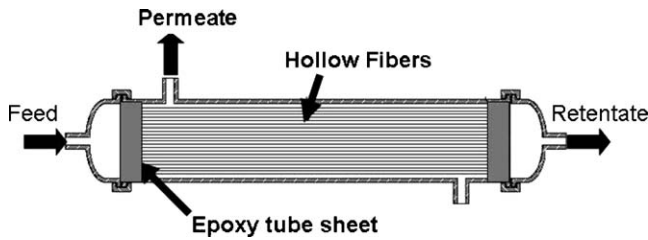*E-mail address:* philippe.moulin@univ-cezanne.fr (P. Moulin).

Fig. 1. Hollow fiber module.

permeates fluxes are mostly analysed using different models: the gel polarization model [6–8], the mass transfer model [9], the osmotic-pressure model [10,11] or the resistance-in-series model [12,13]. The main problem with these models is that they calculate the pressure drop along the membrane using the Hagen–Poiseuille law. This method results in a considerable approximation that could be an important error because the walls are considered as impermeable. There is a significant difference between the results obtained with the Hagen–Poiseuille equation and our results, more particularly for high permeability coefficients. The pressure drop in the membrane could be more than three times higher than the values calculated considering the wall as impermeable. This consideration affects the results of these models. Numerous efforts have been made to model membranes using the CFD approach. Commercial packages are frequently used and the method often consists in resolving the Navier–Stokes and continuity equations for a 2D or 3D steady, laminar flow of an incompressible homogeneous and Newtonian fluid. That is why many recent works have associated membrane processes and computational fluid dynamics [14]. Using CFD, Caroll studied the effect of the properties of the cake and of the fibers on flux declines in hollow fiber microfiltration membranes [15]. The author developed a model for hollow fiber membranes incorporating cake compressibility and demonstrated that the properties of the cake and of the fibers had an effect on the flux decline. Agashichev and Falalejev [16] developed a model giving a quantitative correlation for longitudinal pressure profiles. Their model allows the analysis of the influence of the tangential velocity, transmembrane flux and intrinsic rheological properties of the fluid and channel geometry on the configuration of the pressure profile. Their model, combined with auxiliary sub-models, was segmented and built in algorithm for the longitudinal calculation of the driving force and transmembrane flux. This model is not easy to use, many dimensionless parameters and approximations are involved. On the other hand, Chatterjee et al. [17] developed a numerical solution to model the performance of a radial flow hollow fiber reverse osmosis module. They clearly showed that the two-parameter models used by Sekino [18] may not be adequate for precise design and analysis of many solute–membrane systems. Damak et al. [19] showed that both high axial Reynolds numbers and high Schmidt numbers lead to a decrease in the thickness of the local concentration boundary layer:

$$Re = \frac{\rho v d}{\mu} \tag{1}$$

with ρ the density (kg m^{-3}), v the velocity (m s^{-1}), d the internal diameter (m) and μ is the dynamic viscosity (Pa s):

$$Sc = \frac{\upsilon}{D} \tag{2}$$

with υ the kinematic viscosity (m^2 s^{-1}) and D is the mass diffusivity (m^2 s^{-1}).

In addition, the evolution of the thickness of the local concentration boundary layer for a given wall Reynolds number depends on the values of the Schmidt number and of the axial Reynolds number near the wall:

$$Re_w = \frac{\rho v_w d}{\mu} \tag{3}$$

with v_w the wall velocity (m s^{-1}).

Many authors have tried these processes to model with the maximum of accuracy. Nassehi [20] proposed a general technique for linking the free flow modelled using the Navier–Stokes equations to the flow that passes through the membrane described by the Darcy equation. It can be regarded as the first step towards creating a complete model for cross-flow filtration. Damak et al. [21–23] also worked on this subject and they succeeded in modelling the concentration-polarization phenomena along the membrane under a wide range of operating conditions. Furthermore, numerical simulation can also be used to develop the mass transfer correlation in radial flow hollow fiber modules. In our work, the flow characteristics that control the performance of a hollow fiber membrane module are investigated numerically. The aim of this work is three-fold: determining the pressure drop in a hollow fiber ultrafiltration module under several operating conditions and investigating the effect of various physical parameters on the pressure and velocity profiles along the membrane surface. We propose a simple relation that can estimate the pressure drop as a function of operating and design parameters (permeability, inlet velocity, inlet pressure, channel diameter, etc.). Using the relation, we can deduce the number of clogged fibers and thus control the process. Our work should help to improve the design of the hollow fibers, to anticipate problems such as the clogging of the hollow fibers and/or the module position and to control water production. As a consequence, our work can be used to improve the previous mass transfer models that used the Hagen–Poiseuille law. A good agreement was achieved between the results obtained with our numerical simulation and experimental results.

3. Numerical simulation

In this study, we worked with a commercial CFD package called FLUENT, which is used to simulate the fluid flow in current geometries and to test the influence of the process parameters. The mathematical model consists in solving the Navier–Stokes and continuity equations for a steady, laminar flow of an incompressible homogeneous and Newtonian fluid. In our case, a laminar, incompressible, viscous and isothermal flow in a cylindrical tube with various permeable walls was considered. The geometry considered was axisymmetric (Fig. 2). The simulated domain was 1.3 m in length and up to 2 mm height.
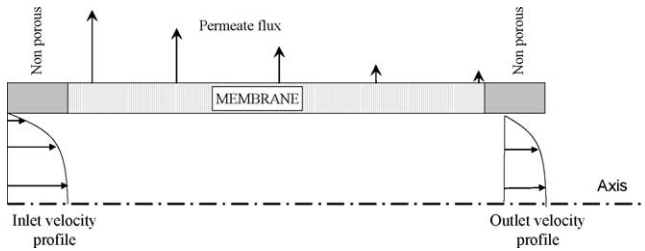
Fig. 2. Representation of the geometry considered.

In order to have an accurate model, we need information about what happens near the membrane surface. So we need a very fine mesh close to the membrane surface. We optimized the grid size to get the best accuracy: 75% of the elements were located close to the membrane. The basic equations of fluid mechanics were combined with the boundary conditions representing a porous wall to simulate the hydrodynamics in a membrane module. The basic equations governing fluid flow are given below.

Continuity equation

$$\nabla \rho V = 0 \tag{4}$$

Momentum transport equation

$$V\nabla(\rho V) = -\nabla P + \mu(\nabla^2 v) \tag{5}$$

For a flow field simulation in a membrane module, the membrane wall can be considered as a semi-permeable surface on which a certain amount of exit flux may be specified. The module is represented as an isothermal steady-state and isolated environment, where only the effects of the laminar flow field within the module contribute to the calculated solution. The feed stream, which flows tangentially to the porous membrane surface, is modelled by the Navier–Stokes equations. All previous equations that were expressed as transport equations are added to the Darcy equation.
Darcy equation

$$J = L_p \, \text{TMP} = \frac{1}{\mu R_m} \text{TMP} \tag{6}$$

with TMP the transmembrane pressure (Pa), J the permeate flux (m s^{-1}), L_p the permeability (m s^{-1} Pa^{-1}), μ the dynamic viscosity (Pa s) and R_m is the membrane resistance (m^{-1}). Pure water is considered during these simulations.
Boundary conditions

The velocity components were fixed at the inlet, with a parabolic profile (fully developed flow), and left free at the outlet. For the feed condition, 5 cm located before and after the membrane were considered as impermeable (plug). The tangential velocity at the surface of the membrane is equal to zero. No equations describing the concentration polarization or fouling phenomena need to be added. For a variable composition feed and/or for an industrial application a simplified mass transfer model cannot be applied in our simulations. Moreover, for an industrial plant, only the variation of the membrane permeability is taken into account. So in this study, the fouling phenomena are considered as a modification of the membrane permeability: it is a simplified approach which can be directly applied for different industrials applications. This simplified approach, no boundary conditions in term of mass transfer equation, was validated hereafter.

The simulations, summarized in Table 1, were done with various values of inlet velocity, inlet pressure, internal diameter and permeabilities. The laminar conditions were always simulated (i.e. Reynolds number less or equal to 2000) and no turbulence conditions were investigated in this paper. The parameter ranges were selected and they are those commonly used in hollow fiber ultrafiltration. The simulated hollow fiber was both horizontal and vertical and mesh refinement enabled us to obtain a good numerical accuracy.

4. Results and discussion

Ultrafiltration in a hollow fiber module with inside-out flow was simulated using a model that takes into account the longitudinal pressure drop. Typical results are presented in Figs. 3 and 4, respectively, variation of the velocity and pressure versus length. The permeability was expressed in L h^{-1} m^{-2} bar^{-1}, as this unit is used in industry. So, with this study, it was possible to obtain the pressure and velocity profiles in membranes (under laminar conditions).

4.1. Mathematical relation

The expression developed for the pressure profile depends on the membrane physical properties and on the process parameters. We used the results obtained by CFD (i.e. pressure drops)
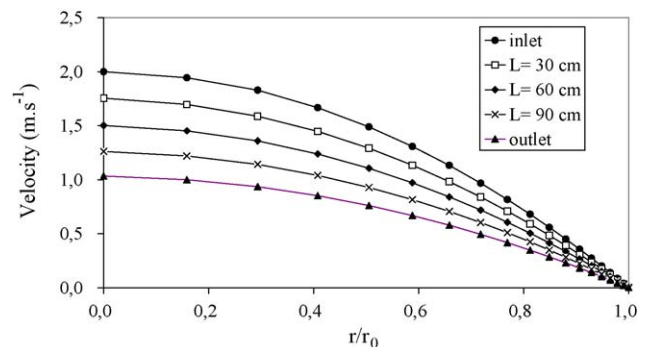
Table 1
Range of simulated operating parameters

Parameter	Range of values
Internal diameter (mm)	[1–2]
Inlet velocity (m s^{-1})	[0, 25–2]
Permeability (L h^{-1} m^2 bar^{-1})	[100–800]
Inlet pressure (kPa)	[50–150]
Reynolds number	[250–2000]

Fig. 3. Representation of the gradient velocity on the half of the channel at different channel positions ($L_p = 800 \, \text{L h}^{-1} \, \text{m}^{-2} \, \text{bar}^{-1}$, $v = 1 \, \text{m s}^{-1}$, $d = 1$ mm, $P_i = 100$ kPa, $L = 1.2$ m).
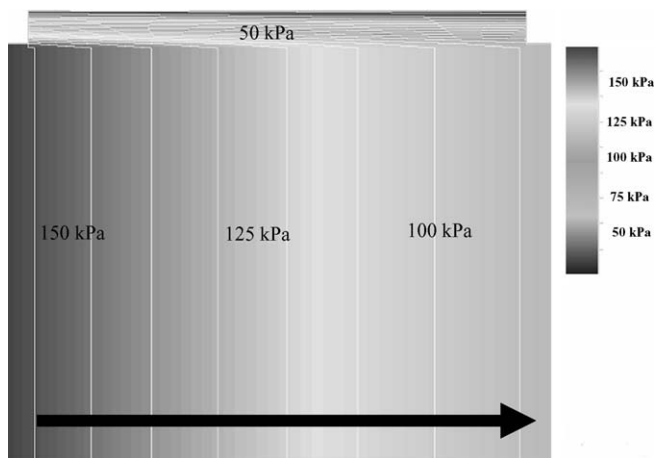
Fig. 4. Representation of the pressure along the membrane ($L_p = 800$ L h^{-1} m^{-2} bar^{-1}, $v = 1$ m s^{-1}, $d = 1$ mm, $P_i = 150$ kPa, $L = 1.2$ m).

and the solver add-in of Excel to create a relation linking the pressure drop to all the variables. The solver add-in can adjust the power law of each parameter such as it minimizes the sum of the differences between the pressure drops obtained by CFD and by the formula. The model equation proposed for a horizontal hollow fibber position is

$$\frac{\Delta P}{L} = \frac{0.15 v^{1.17}}{L_p^{0.15}(P_i \times 10^{-3})^{0.2} d^2} \qquad (7)$$

with P_i the inlet pressure (Pa), ΔP the pressure drop (Pa), L_p the permeability (L h^{-1} m^{-2} bar^{-1}), L the membrane length (m), d the membrane diameter (m) and v is the mean velocity at the inlet of the feed channel (m s^{-1}). The validation range of this model equation is given by Table 1. The range of operating parameters is adapted for ultrafiltration applications. For example it is impossible to calculate the pressure drop for a no permeable tube. This equation relating the pressure drop with membrane permeability parameters pertaining to fiber dimensions, feed inlet, pressure and feed flow velocity is a very important result.

Many numerical simulations were run to show the high flexibility of this relation. There was a good agreement between the relation and the numerical simulation: the difference between the pressure drop value obtained by CFD and those obtained by the relation was lower than 2% (Fig. 5). We consider that this relation is suitable when the permeate flow is less than 70% of the inlet flow. Moreover, an interesting consideration was taken in account in this part: the influence of the hollow fiber module position. In fact, two positions could be required for these processes: vertical and horizontal. The vertical configuration was also studied, since one finds as well processes used in vertical position as horizontal. The difference with the relation previously established is equal to the water column height and the permeability does not have any influence.

4.2. Effect of the inlet velocity

Filtration resistance caused by the concentration polarization and the reversible fouling layer significantly decreases with
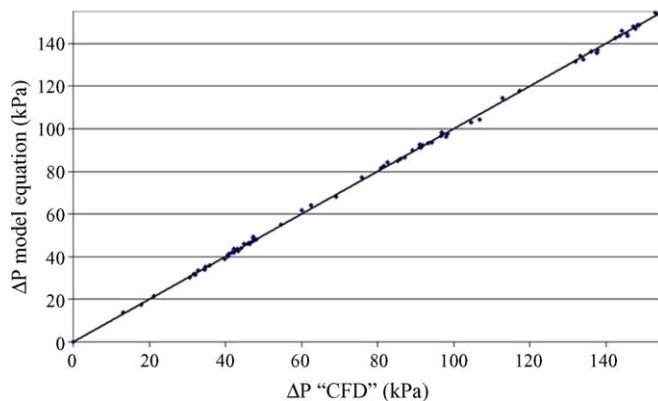

Fig. 5. Comparison between the results obtained by CFD and the results obtained using relation (7) for the operating variable ranges given in Table 1.

increasing cross-flow velocity. It is clearly expected that as cross-flow velocity increases, the mass and the thickness of the fouling layer should decrease, resulting in decreased filtration resistance. It is also well known that if we increase the axial velocity in our membrane, the pressure drop increases, as shown in Fig. 6. The pressure loss is around twice as significant when the inlet velocity increases from 1 to 2 m s^{-1}. In the case of impermeable tubes, the dependence is more significant. More the permeability is high, more the permeation attenuates the effect of the inlet velocity. In fact, the permeation reduces the flow rate along the membrane and reduces the pressure drop and the velocity [25].

4.3. Effect of the membrane permeability and inlet pressure

Membrane permeability and inlet pressure are used to determine the permeate flux which is directly proportional to membrane porosity and/or membrane fouling. Therefore, we can assume that the pressure drop is greater with higher inlet pressure. Fig. 7 shows the results obtained. The pressure drop is 30% less significant at 150 kPa than at 50 kPa at the same Reynolds number (1000). This observation should be taken into account to improve hollow fiber ultrafiltration processes. The transmembrane pressure difference is the driving force that controls the permeate flux. Fig. 8 shows the influence of the permeability
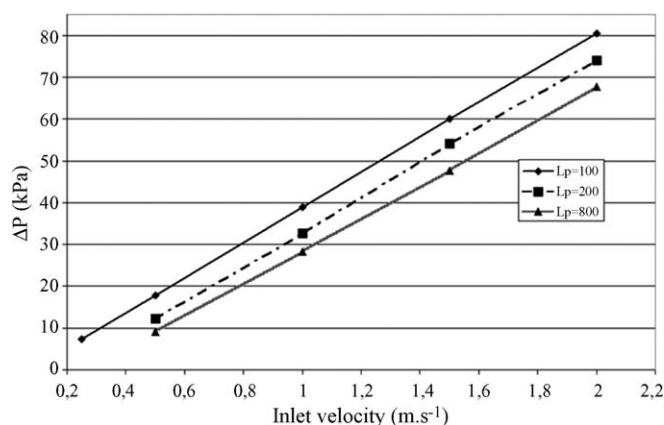

Fig. 6. Variation of the pressure drop as a function of the inlet velocity for different permeability values (L h^{-1} m^{-2} bar^{-1}) ($P_i = 100$ kPa, $d = 1$ mm, $L = 1.2$ m).
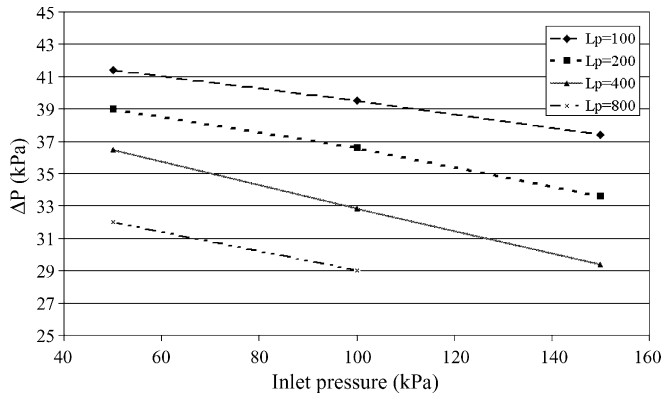
Fig. 7. Variation of the pressure drop as a function of the inlet pressure for different permeability values ($L\,h^{-1}\,m^{-2}\,bar^{-1}$) ($d = 1\,mm$, $L = 1.2\,m$, $v = 1\,m\,s^{-1}$).

Fig. 9. Variation of the pressure drop along the membrane as a function of the membrane length for different permeability values ($L\,h^{-1}\,m^{-2}\,bar^{-1}$) ($P_i = 100\,kPa$, $d = 1\,mm$, $L = 1.2\,m$, $v = 1\,m\,s^{-1}$).

on the pressure drop for different inlet pressure. The pressure drop is lower when the friction resistance declines and naturally when the permeability increases. Therefore, the outlet pressure decreases when the porosity of the porous media decreases and when the inlet velocity increases. From the results of the numerical simulations, we can thus estimate the pressure drops in permeable hollow fibers under the standard hollow fiber use condition. We could verify that the more the velocity increases and the inlet pressure decreases, the more the pressure drop along the membrane increases. We could also verify that an increase in the permeability, or in the membrane diameter, results in a decrease in the pressure drop. All of these parameters can be quantified using this relation.

4.4. Effect of membrane length and position

We now consider the effects of the membrane length. Numerical simulation results were compared with other results obtained using a classical relation (Fig. 9). Other authors have calculated the pressure drop in a membrane module using the Hagen–Poiseuille law. Vladisavljevi and Mitrovi [24] developed a relation for calculating the pressure drop in a hollow fiber derived from the Hagen–Poiseuille law. They expressed the total pressure drop as being equivalent to the pressure drop
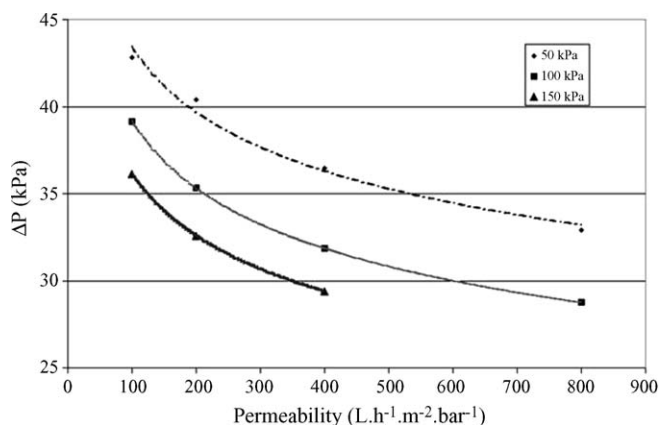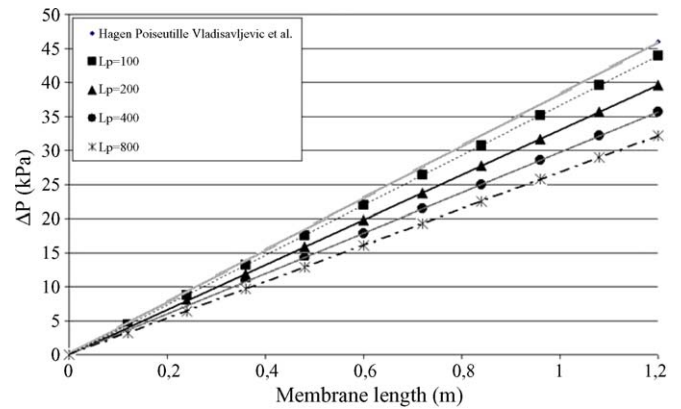
due to the friction resistance added to the pressure drop due to local resistances in the module. In this paper, we well verify that the pressure drop increases when the inlet velocity increases. So, when the inlet velocity increases we can estimate that the friction coefficient increases and that the pressure drop increases along the membrane. However, for high permeabilities, the flow passes through the membrane easily and the permeate flow is higher. That is the reason why the pressure drops decreases and could become twice as low as that calculated with the Hagen–Poiseuille equation. These considerations are in agreement with the results presented in this paper. As expected, an increase in water flow rate, fiber length and diameter, and permeability influences significantly energy losses in the module. We also verified that the pressure drop was quasi-linear along the whole membrane length. The values of the pressure in the channel all along the channel for different permeabilities are reported in Fig. 10. In porous conditions, the pressure drop along the membrane could be considered as linear for low permeability studied. As a result, the approximation made in the relation has no consequence on the accuracy of the model. Our model gives a quantitative correlation for a longitudinal pressure profile.
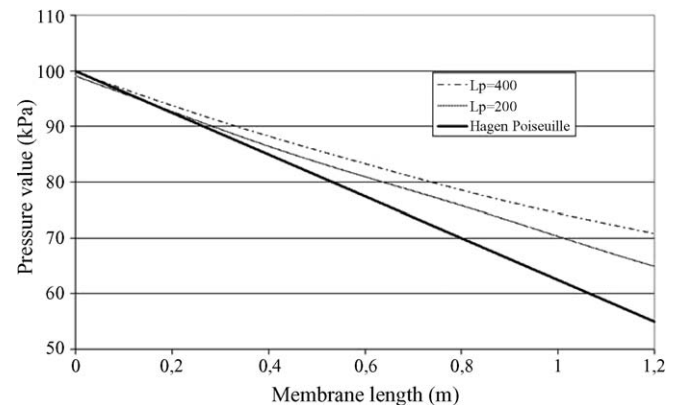

Fig. 8. Variation of the pressure drop as a function of the permeability at different inlet pressure values ($v = 1\,m\,s^{-1}$, $d = 1\,mm$, $L = 1.2\,m$).

Fig. 10. Variation of the pressure value along the membrane as a function of the membrane length for different permeability values ($L\,h^{-1}\,m^{-2}\,bar^{-1}$) ($P_i = 100\,kPa$, $d = 1\,mm$, $v = 1\,m\,s^{-1}$).

Let us now consider the influence of the position of the hollow fiber system. In fact, two positions are possible: vertical or horizontal. To assess the influence of the membrane position, we ran the same number of simulations as before with a vertical and a horizontal membrane using the same parameters and for a total membrane length fixed at 1.3 m. The pressure difference between the two results (vertical and horizontal membrane) is 13 kPa ± 5%. This value is due to the weight of the water in the module and the percentage is function of the parameter studied. Therefore, the pressure drop in the module could easily be determined with our relation in both cases. In fact, the difference of pressure could be calculated with the Bernouilli relation.

This difference of pressure given by the Bernouilli relation added to our relation gives the correct pressure drop in the case of a vertical membrane.

Moreover, the model allows the analysis of the influence of the tangential velocity, transmembrane flux and channel geometry on the pressure profile configuration. This relation can be used in many applications, in particular in "process maintenance". This relation has multiple advantages: it enables us to quickly determine the integrity of a module, to calculate the influence of each variable on the pressure drop with/without fouling (i.e. membrane permeability) and to evaluate the energy consumption.

4.5. Determination of the percentage of clogged hollow fibers

In fact, we just need to calculate the flow that circulates in one hollow fiber. If one hollow fiber is clogged, the velocity will increase in all the other fibers and so will the pressure drop along the module. For a constant value of the inlet pressure and inlet flow rate, the effect of the number of clogged hollow fibers on the pressure drop can be estimated as shown in Fig. 11. During the process operation, by increasing the manometer precision, it will be possible to determine the percentage of clogged hollow fibers without stopping the process.
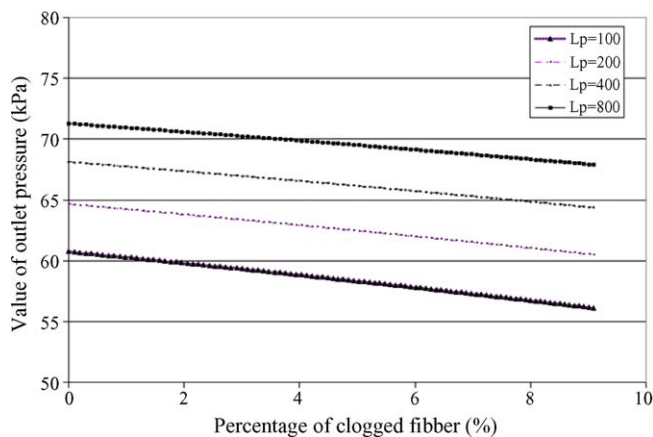

Fig. 11. Variation of the outlet pressure value as a function of the percentage of clogged hollow fibers for different permeability values (L h^{-1} m^{-2} bar^{-1}) (L_p = 100, 200, 400 and 800 L h^{-1} m^{-2} bar^{-1}, P_i = 100 kPa, d = 1 mm, L = 1.2 m, Q_{inlet} = 100 m^3 h^{-1}, 35,000 hollow fibers).
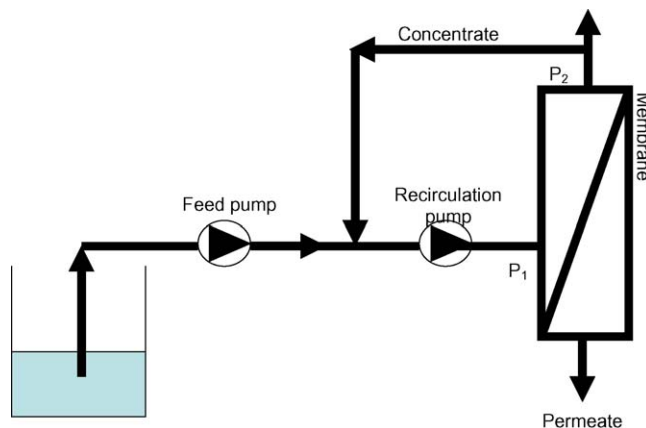

Fig. 12. Industrial-scale plant used for energy calculations.

4.6. Energy consumption

The application of the proposed Eq. (7) could also allow energy considerations. A calculation was performed in order to estimate the energy consumption of the ultrafiltration process. The pump power can be divided into feed pump power and recirculation power, as in the industrial-scale plant shown in Fig. 12. The feed pump power, W_{feed} (W) can be expressed as

$$W_{feed} = JS(P_2) \tag{8}$$

with J the permeate flow (m s^{-1}), S the membrane area (m^2) and P_2 is the pressure at module outlet (Pa).

The circulation power, W_{circ} (W) can be expressed as

$$W_{circ} = Q_{circ}(P_1 - P_2) \tag{9}$$

with Q_{circ} the average circulation flow rate (m^3 s^{-1}) and P_1 and P_2, respectively, the pressures at the inlet and the outlet of the module (Pa). Then a total power W_{tot} is calculated as the sum:

$$W_{tot} = W_{feed} + W_{circ} \tag{10}$$

and E_c, the energy consumed per m^3 of permeate produced (Wh m^{-3}) is given by

$$E_c = \frac{W_{tot}}{JS} \tag{11}$$

Consequently, the energy consumption can be calculated and our relation (7) can be interesting from an energetic point of view. For example, the pressure drop in the module influences the recirculation pump power and the energy required to maintain the same average circulation flow rate. In fact, the term $P_1 - P_2$ represents the pressure drop along the membrane. This term can be calculated using the equation. Moreover, we can deduce the influence of the percentage of clogged hollow fibers on the energy consumption. Therefore, for a constant inlet pressure and a constant feed flow, the energy consumed per cubic metre of permeate produced during the process increases gradually to maintain the same permeate flux. We can thus quantify this power required during the process, as shown in Fig. 13. We can notice that the percentage of clogged fibers plays a very significant role in the energy consumption during the process.
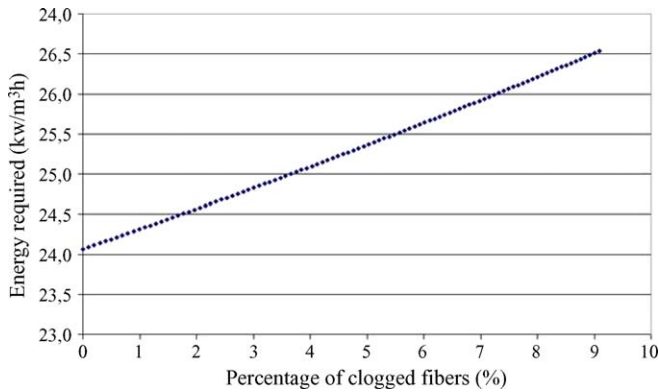
Fig. 13. Variation of required pump power as a function of the percentage of clogged hollow fibers ($L_p = 100 \, L \, h^{-1} \, m^{-2} \, bar^{-1}$, $v = 1 \, m \, s^{-1}$, $P_i = 150 \, kPa$, $d = 1 \, mm$, $L = 1.2 \, m$, $Q_{inlet} = 200 \, m^3 \, h^{-1}$, 35,000 hollow fibers).

The pressure drop increases with the time and to compensate this phenomenon, we have to increase the recirculation force in order to maintain the same permeate flux. As a result, we can see that this required energy can increase by more than 7% if 10% of the hollow fibers are clogged. This increase is not negligible because the energy consumption in these kinds of processes is already very high. This parameter should also be taken into account to improve membrane processes.

5. Comparison between experiment data and the model

We did not simulate the pressure drop at the inlet and the outlet of the module. The pressure drop can be either calculated using a classical hydrodynamic formula given in the literature or measured. The singular pressure drop can be determined by the application of the following formulas which take into account the local resistances such as the changes of section, abrupt or progressive widening of the channel and presence of a valve:

$$\Delta P = \tau \frac{\rho \bar{v}^2}{2} \tag{12}$$

τ is a dimensionless coefficient that is determined for each case of structure change and $\bar{v}$ is the mean velocity in the element considered ($m \, s^{-1}$).

Therefore, the sum of the pressure drops calculated could be compared to the value given by the manometers positioned along the process line. Therefore, the two pressure drops could easily be coupled using this method. In our case, the simulation results were compared with experimental results. The pressure drop was obtained by the difference between the inlet pressure and the outlet pressure given by two manometers positioned in an industrial pilot plant. This pilot plant was automated, operated under industrial conditions and contained a hollow fiber module ($7 \, m^2$). Natural water from the "Canal de Provence" was used as feed by the pilot plant located at Bouc Bel Air, near Marseilles (France). This water was pumped with a feed pump and screened with a $300 \, \mu m$ pre-filter. A cross-flow filtration mode was used. This pilot plant was automatically controlled in order to keep the permeate flux constant. Hollow fiber membranes with a M.W.C.O (molecular weight cut off) of $100 \, kDa$
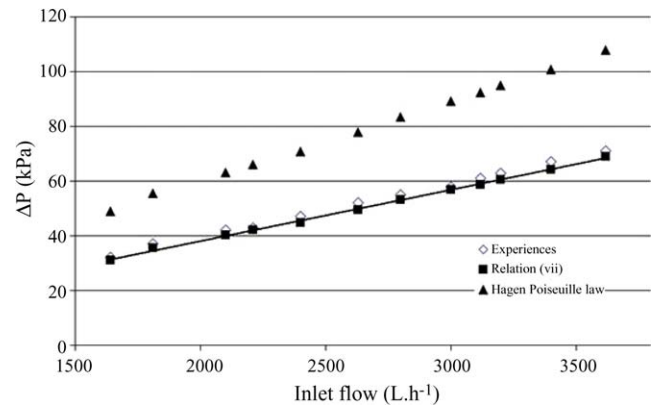

Fig. 14. Comparison of pressure drops for different inlet velocities obtained through experiments and numerical simulations ($T = 20 \, °C$, turbidity < 5 NTU, $L_p = 200 \, L \, h^{-1} \, m^{-2} \, bar^{-1}$, $\Delta P_i = 50–90 \, kPa$, $v = 0.2–1.5 \, m \, s^{-1}$, $L = 1.2 \, m$, $n = 2000$ fibers $d_i = 0.93 \, mm$).

were used. The module contained 2000 fibers 0.93 mm in inside diameter. The membrane permeability was $200 \, L \, h^{-1} \, m^2 \, bar^{-1}$. The range of experiments used to validate our results was the same as before. Therefore, the circulation flows ranged between l600 and $3800 \, L \, h^{-1}$, and the inlet velocities ranged between 0.2 and $1.5 \, m \, s^{-1}$. The comparison of experimental results and simulation results (Fig. 14) validates our relation. The percentage of error between relation and experiment was less than 2%. This error could be due to the precision of the two manometers. A large number of tests covering typical ultrafiltration applications have demonstrated that the model describes the pressure loss in hollow fiber processes. Our relation may be used in many applications and may help to improve the accuracy of existing models and to optimize membrane processes.

In this study, any boundary condition and more especially mass transfer model are not used to describe the membrane fouling. The membrane permeability decreases when the membrane fouling increases (Fig. 15) for a constant permeate flux. This figure represents the variation of the permeability during experiences for a constant permeate flux equal to $110 \, L \, h^{-1} \, m^{-2}$. During each filtration step, for example in the case of drinking water production, it was possible to predict the pressure drop
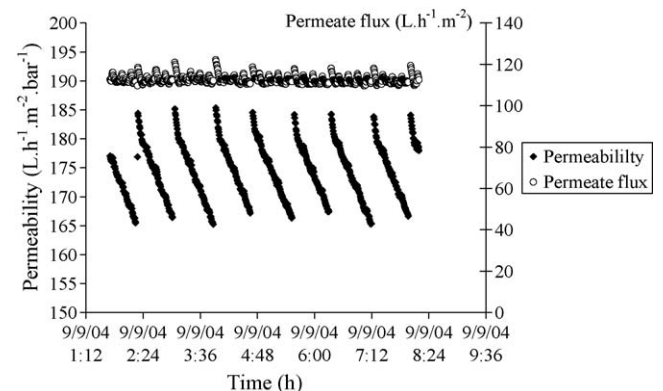

Fig. 15. Variation of the permeate flux and the permeability vs. time ($T = 20 \, °C$, $J = 114 \, L \, h^{-1} \, m^{-2}$, $v = 0.7 \, m \, s^{-1}$, $L = 1.2 \, m$, $n = 2000$ fibers, $d_i = 0.93 \, mm$).
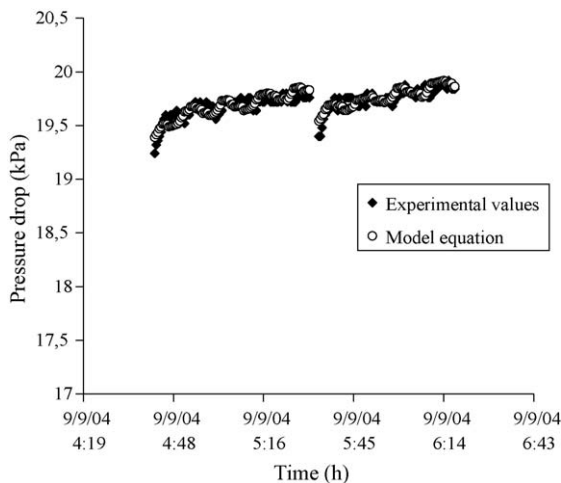
Fig. 16. Variation of the pressure drops (experimental values and simulation) vs. time ($T = 20\,°C$, $J = 114\,L\,h^{-1}\,m^{-2}$, $v = 0.7\,m\,s^{-1}$, $L = 1.2\,m$, $n = 2000$ fibers, $d_i = 0.93\,mm$).

with the variation of the membrane permeabilities whatever the fouling by our model equation (Fig. 16): a good agreement was obtained.

6. Conclusion

A simple relation representing the flow mechanism in a hollow fiber ultrafiltration process was proposed to calculate the pressure drop. Various simulations were run to show the flexibility of this relation for a wide range of inlet velocities, inlet pressures, internal diameters, permeabilities. We determined the influence of each of these parameters and more particularly of the operating parameters and of the membrane characteristics. We obtained the pressure and velocity profiles for different conditions. This equation relating the pressure drop with membrane permeability, parameters pertaining to fiber dimensions, feed inlet, pressure and feed flow velocity are a very important result.

Moreover, the numerical simulations were realistic and corresponded to the traditional use of hollow fiber ultrafiltration membranes. This relation was compared with the results obtained using an industrial pilot plant. A good agreement was obtained with the experimental results and allowed us to check the integrity of the module. Any boundary condition and more especially mass transfer model are used to describe the membrane fouling. The membrane permeability decreases when the membrane fouling increases for a constant permeate flux. During each filtration step, for example, in the case of drinking water production, it was possible to predict the pressure drop whatever the fouling by our model equation: a good agreement was obtained.

Therefore, we can deduce the percentage of clogged hollow fibers and evaluate energy consumption by calculating the pressure drop. With our relation, we can determine the pressure drop with high accuracy. We can also improve the accuracy of previous models developed for membrane processes. Additional numerical simulations could be run to improve the existing mod-

els by calculating the pressure drop at the inlet and the outlet of the module.

References

[1] S. Veríssimo, K.-V. Peinemann, J. Bordado, New composite hollow fiber membrane for nanofiltration, Desalination 184 (2005) 1.

[2] A. Broeckmann, J. Busch, T. Wintgens, W. Marquardt, Modeling of pore blocking and cake layer formation in membrane filtration for wastewater treatment, Desalination 189 (2006) 97.

[3] A.-S. Berman, Laminar flow in channels with porous walls, J. Appl. Phys. 24 (1953) 12.

[4] A.-S. Berman, Effects of porous boundaries on the flow of fluids in systems with various geometries, in: Proceedings of the Second United Nations International Congress on the Peaceful Use of Atomic Energy, vol. 4, 1958, p. 358.

[5] S.-W. Yuan, A.B. Finkelstein, Laminar flow with injection and suction through a porous wall, Trans. ASME 78 (1956) 719.

[6] M.-J. Clifton, N. Abidine, P. Aptel, V. Sanchez, Growth of the polarization layer in ultrafiltration with hollow-fiber membranes, J. Membr. Sci. 21 (1984) 233.

[7] H.-M. Yeh, T.-W. Cheng, Concentration polarization model for hollow fiber membrane ultrafiltration, Sep. Sci. Technol. 29 (1994) 497.

[8] H.-M. Yeh, Modified gel-polarization model for ultrafiltration in hollow-fiber membrane modules, Sep. Sci. Technol. 31 (1996) 201.

[9] T. Kotzev, Numerical study of the fluid dynamics and mass transfer of an ultrafiltration performance in a tube membrane module, Int. J. Eng. Sci. 32 (1994) 359.

[10] H.-M. Yeh, T.-W. Cheng, Osmotic-pressure model with permeability analysis for ultrafiltration in hollow fiber membrane modules, Sep. Sci. Technol. 3 (1993) 91.

[11] H. Nabetani, M. Nakajima, A. Watanabe, S. Nakao, S. Kimura, Effects of osmotic pressure and adsorption on ultrafiltration of ovalbumin, AIChE J. 36 (1990) 907.

[12] H.-M. Yeh, T.-W. Cheng, Resistance in series for membrane ultrafiltration in hollow fibers of tube-and-shell arrangement, Sep. Sci. Technol. 28 (1993) 1341.

[13] M. Yeh, H.-P. Wu, J.-F. Dong, Effects of design and operating parameters on the declination of permeate flux for membrane ultrafiltration along hollow-fiber modules, J. Membr. Sci. 213 (2003) 33.

[14] R. Ghidossi, D. Veyret, P. Moulin, Membrane and computational fluids dynamics: state of the art and opportunities, Chem. Eng. Proc. 45 (2006) 437.

[15] T. Carroll, The effect of cake and fiber properties on flux declines in hollow-fiber microfiltration membranes, J. Membr. Sci. 189 (2001) 167.

[16] S.-P. Agashichev, D.-V. Falalejev, Modelling driving force in processes of ultrafiltration of non-Newtonian fluids, J. Membr. Sci. 171 (2000) 73.

[17] A. Chatterjee, A. Ahluwalia, S. Senthilmurugan, S.-K. Gupta, Modelling of a radial flow hollow fiber module and estimation of model parameters using numerical techniques, J. Membr. Sci. 236 (2004) 1.

[18] M. Sekino, Study of an analytical model for hollow fiber reverse osmosis module systems, Desalination 100 (1996) 85.

[19] K. Damak, A. Ayadi, P. Schmitz, B. Zeghmati, Modeling of crossflow membrane separation processes under laminar flow conditions in tubular membrane, Desalination 168 (2004) 231.

[20] V. Nassehi, Modelling of combined Navier–Stokes and Darcy flows in crossflow membrane filtration, J. Chem. Eng. 53 (1998) 1253.

[21] K. Damak, A. Ayadi, B. Zeghmati, P. Schmitz, A new Navier–Stokes and Darcy's law combined model for fluid flow in crossflow filtration tubular membranes, Desalination 161 (2004) 67.

[22] K. Damak, A. Ayadi, P. Schmitz, B. Zeghmati, Modeling of crossflow membrane separation processes under laminar flow conditions in tubular membrane, Desalination 168 (2004) 231.

[23] K. Damak, A. Ayadi, P. Schmitz, B. Zeghmati, Concentration polarisation in tubular membranes: a numerical approach, Desalination 171 (2005) 139.

[24] G.-T. Vladisavljevic, M.V. Mitrovi, Pressure drops and hydraulic resistances in a three-phase hollow fiber membrane contactor with frame elements, Chem. Eng. Proc. 40 (2001) 3.

[25] R. Moll, Etude de l'amélioration des performances membranaires par des vortex de Dean, Thesis no. 2005AIX30028, Université Paul Cezanne Aix Marseille III (2005).